ISSN 0020-1685, Inorganic Materials, 2007, Vol. 43, No. 9, pp. 956–963. © Pleiades Publishing, Inc., 2007.
Original Russian Text © S.A. Kulinich, M. Farzaneh, X.W. Du, 2007, published in Neorganicheskie Materialy, 2007, Vol. 43, No. 9, pp. 1067–1075.

Growth of Corrosion-Resistant Manganese Oxide Coatings on an Aluminum Alloy

S. A. Kulinich[a], M. Farzaneh[a], and X. W. Du[b]

[a] *CIGELE/INGIVRE, Université du Québec à Chicoutimi, Saguenay, PQ, Canada G7H 2B1*

[b] *School of Materials Science and Engineering, Tianjin University, Tianjin 300072, People's Republic of China*
e-mail: s_kulinich@yahoo.com

Received December 29, 2006

Abstract—Data are presented on the nucleation and growth of corrosion-resistant manganese-oxide-based films on the surface of aluminum alloy 2024 in an alkaline $KMnO_4$ solution at room temperature and elevated temperatures, which accelerate film growth. We consider the morphological evolution of the films and second-phase particles present on the alloy surface, which impair the corrosion resistance of the alloy. Also addressed are the feasibility of MnO_4^- incorporation into the growing film and the associated ability of the coating to self-heal when slightly damaged. Such coatings are a viable alternative to chromate-based coatings, which are currently in wide use.

DOI: 10.1134/S0020168507090087

INTRODUCTION

Chromate conversion coatings (CCCs), produced by exposing the alloy surface to aqueous chromate solutions, have now been successfully used to protect various aluminum alloys from corrosion for several decades [1–8]. At the same time, since Cr(VI) compounds are carcinogenic, intensive research effort has been concentrated on chromate-free systems in order to gradually replace chromates and related coatings in large-scale applications [2, 3, 9–14]. One alternative approach is to produce coatings by oxidizing aluminum with the permanganate anion, followed by Mn(IV) deposition. Permanganate conversion coatings (PCCs) thus grown already find some industrial applications [15–21].

There have been several reports that the permanganate ion is not effective in preventing corrosion on the surface of Al alloys at low pH values [2, 22]. At the same time, at high pH values MnO_4^- is capable of inhibiting the corrosion of Al-based alloys [22], which is probably due to the fact that the reduction of Mn(VII) in alkaline media typically leads to the formation of MnO_2, a less soluble species [23]. Bibber [15–18] proposed and patented a process for producing stable $KMnO_4$-based conversion coatings on a variety of Al alloys. The first implementation of that process required multiple treatments with various salt solutions (the last step was immersion in a $KMnO_4$ solution), typically at elevated temperatures, and the resultant coatings were somewhat inferior in corrosion protection properties to CCCs [2, 15]. Optimization of the process, however, made it possible to reduce the number of steps (by combining several solutions into one) and to reach corrosion resistance close to that of CCCs [16–18]. The recommended range of process temperatures is 38–82°C, and the solution pH must lie between 9 and 10 [16]. At lower temperatures, the process takes a longer time, up to 60 min at room temperature, whereas at 68°C a coating can be formed in ≃1 min [16]. To apply high-quality corrosion-resistant coatings to Cu- or Zn-rich alloys, an additional step is necessary, treatment in a silicate solution, which blocks process-induced defects and cracks in the coating [18]. The coatings thus formed are very close in performance to CCCs [18]. Moreover, PCCs offer the advantage of higher thermal stability [18]. Also important is that permanganates, which have long been used to purify drinking water, are attractive for large-scale application, in contrast to Cr(VI) compounds [18]. However, in spite of the considerable potential of PCCs as a safe alternative to CCCs and the reports that they can be successfully used to protect Al alloys [15–21], the growth and properties of such coatings are essentially unexplored, which limits their practical application.

The capability of some conversion coatings for active corrosion protection (ACP) is of considerable practical importance. It is now well documented that such behavior is offered by CCCs, which contain some amount of chromate anions capable of migrating to local sites of mechanical damage and oxidizing them, thereby restoring the corrosion protection [4, 6–8, 10]. Such processes were also observed in vanadate [12] and cerium-oxide-based (containing Ce(III) and Ce(IV) oxides) [10] conversion coatings. The question of whether MnO_4^- anions are incorporated in PCCs has already been addressed in the literature [18, 19]. The

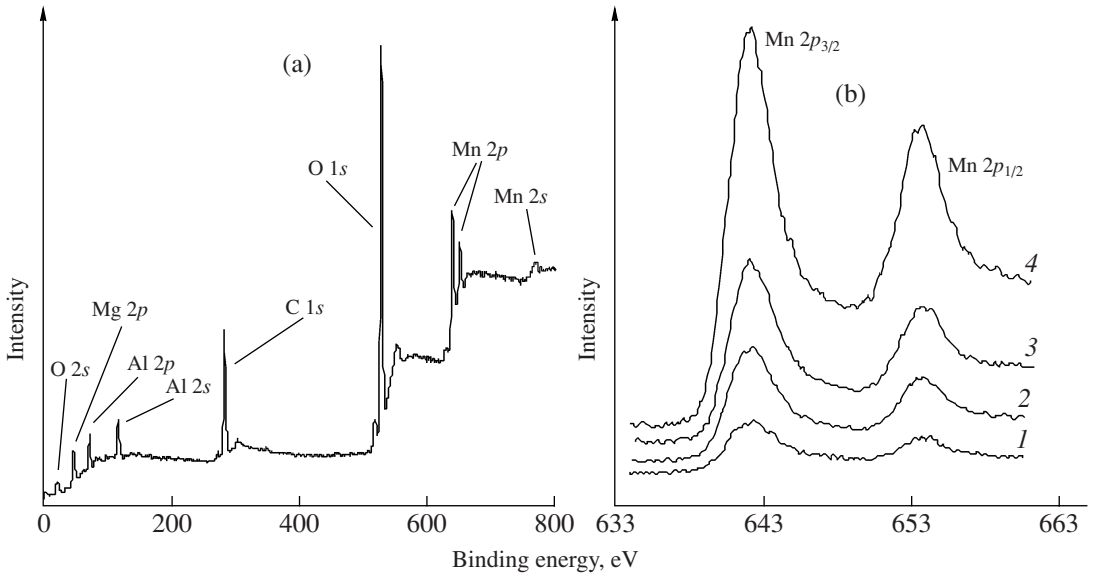

Fig. 1. (a) XPS survey scan of AA2024 treated at room temperature for 60 min; (b) Mn 2*p* spectra of samples treated for (*1*) 5, (*2*) 20, (*3*) 60, and (*4*) 150 min.

presence of MnO_4^- on sample surfaces was confirmed by IR spectroscopy, but no in-depth studies were carried out [18, 19].

In this paper, we focus on several important aspects of the growth of conversion films from alkaline an $KMnO_4$ solution: (1) the effect of intermetallic second-phase inclusions on the initial stages of growth, (2) later stages of growth and coating morphology, (3) effect of solution temperature, and (4) feasibility of MnO_4^- incorporation into the coating in the context of ACP.

EXPERIMENTAL

Aluminum alloy 2024 plates were polished to mirror finish (using 1-μm diamond slurry in the final step) and cleaned by sonication in acetone and methanol. In permanganate conversion treatment, we used a two-component solution containing 0.1 M $KMnO_4$ and 0.05 M $Na_2B_4O_7$. The solution pH was ≈9.1, and the solution composition was close to one of the formulations proposed by Bibber [16, 17]. The same $KMnO_4$ concentration was used earlier by Danilidis et al. [19, 20]. AA2024 samples were immersed in the reaction solution and kept in it for a certain period of time with constant stirring. Next, the samples were washed with distilled water and dried in air.

The formation of PCCs on Al alloys is known to be a slower process compared to the formation of CCCs, which is close to completion after several minutes at room temperature [1, 4, 24, 25]. PCC growth can be accelerated by raising the temperature [16, 18]. Note that elevated temperatures in the range 40–70°C were also used in permanganate and permanganate–phosphate conversion treatments of Mg alloys [26–30]. In view of this, several samples were conversion-treated at 50 and 68°C for 3 min, in contrast to the other samples, which were treated at room temperature.

In different stages of growth, the samples were characterized by scanning electron microscopy (SEM) and energy-dispersive x-ray spectroscopy (EDS) on a Philips XL30E, x-ray photoelectron spectroscopy (XPS) (Physical Electronic Industries PHI-1600 spectrometer), and Auger electron spectroscopy (Thermo Electron Microlab 350, spot size down to about 12 nm) [7, 8].

RESULTS AND DISCUSSION

XPS and chemical composition. The chemical composition of the coatings was determined by XPS in different stages of growth. Figure 1a shows the XPS spectrum of a sample treated for 60 min. In accordance with an earlier study [19], where the major component of PCCs was MnO_2, our films were composed predominantly of Mn and O. In addition, as can be seen from Fig. 1a, the surface layer (≈10 nm) of the sample contained Al and Mg. Significant levels of Al were only found in samples treated for no longer than ≈90 min. Since no Al was detected by XPS after 90 min of treatment, the presence of Al in the coatings appears unlikely. Presumably, in this stage (<90 min) the coatings consisted of isolated islands or had regions ≤10 nm in thickness, so that XPS probed the surface layer of the AA2024 substrate. It will be shown below that, in such regions, the coating began to grow later and was thinner in comparison with the rest of the coating. On the other hand, XPS data indicated that the incorporation of aluminate ions, detected in earlier studies [18, 19], into our coatings was insignificant.

Since Cu (trace amounts) was detected in the surface layer of the samples only after short-term (1 and 5 min) treatment, it is reasonable to assume that a small amount of Cu was present at the substrate/coating interface, whereas the copper content in the bulk of the PCCs was below the detection limit of XPS, as was the boron content. After 90 min of treatment, the Al peaks in the XPS spectra disappeared, giving way to K and Na peaks. Together with Mg, which was not detected in the initial stage of growth, these elements were the major impurities in our PCC coatings. K and Na were present in the permanganate bath, whereas the Mg incorporation was due to dissolution of the top layer of the substrate and subsequent precipitation of the material from the solution. It is, however, unclear how K, Na, and Mg were incorporated into the PCC in later stages of growth, whereas Cu and Al, whose concentrations in the solution were comparable to the Mg concentration, were not detected as inclusions. After 150 min of treatment, the XPS spectra remained essentially unchanged, which suggests that, after ≃150 min of exposure to the $KMnO_4$ solution at room temperature, the conversion layer stops growing.

According to a Pourbaix diagram [25], the native oxide on Al is unstable in the alkaline medium used in this study (pH ≃ 9.1) and dissolves in the aqueous solution according to the scheme

$$Al_2O_3 + 2OH^- + 3H_2O = 2Al(OH)_4^-. \quad (1)$$

The oxidation of the metal and reduction of Mn(VII) to Mn(IV) can be represented by

$$Al + MnO_4^- + 2H_2O = Al(OH)_4^- + MnO_2. \quad (2)$$

Danilidis et al. [19] identified both products of reaction (2) (MnO_2 and $Mn(AlO_2)_2$) in PCCs, but the present XPS data provide no evidence for the presence of aluminates in PCCs. Presumably, this discrepancy is related to the coating processes used: Since Danilidis et al. [19] produced conversion films through reaction of a thin $KMnO_4$ solution layer with the alloy surface during annealing (no-rinse technique), without immersing the alloy in the solution, dissolution of the resulting aluminates was ruled out.

Figure 1b shows the Mn 2*p* XPS spectra of four samples treated in a permanganate bath at room temperature for 5, 20, 60, and 150 min. Even careful analysis of the spectra in Fig. 1b in comparison with literature data gives no way of concluding that coatings contain a significant amount of MnO_4^- ions. The spectra show no Mn(VII) peaks in the binding energy range corresponding, according to several reports [31–34], to Mn $2p_{3/2}$: ≃645.8–647.2 eV. The strongest Mn $2p_{3/2}$ peak, the one at ≃643 eV, is most likely due to manganese(IV) oxide, a major component of the coatings, but the presence of manganese(III) oxide also cannot be ruled out because these oxides are close in Mn $2p_{3/2}$ binding energy (642.4 and 643.0 eV for Mn(III) and Mn(IV), respectively [31]). At the same time, a large amount of Mn_2O_3 would be in conflict with earlier results for PCCs on Al alloys [18, 19, 25].

The Mn 2*p* spectra of the samples prepared at elevated temperatures were similar to those in Fig. 1b and also indicated that the coatings contained insignificant amounts of permanganate anions. Thus, our results lead us to conclude that the MnO_4^- concentration in the bulk of our PCCs is below the detection limit of XPS. In connection with this, the IR absorption peaks of surface MnO_4^- reported by Danilidis et al. [19] are, most likely, attributable to the fact that their samples were not washed and could contain unreacted $KMnO_4$. Since Bibber [18] did not describe the preparation of the sample which was also reported to contain MnO_4^- in the surface layer, its origin remains unclear. One possible reason for the insignificant incorporation of Mn(VII) into PCCs is that they do not have a so-called "inorganic polymer" structure [18], which is well documented for CCCs and is, in many respects, associated with the formation of unique covalent bonds, Cr(VI)–O–Cr(III), in the coatings [6].

Initial stage of growth. The vast majority of intermetallic inclusions in AA2024 are either Al–Cu–Mg or Al–Cu–Fe–Mn particles [5, 7, 8, 24, 35, 36]. The particles of the former kind are usually thought to have the composition Al_2CuMg; the composition of the latter particles is believed to be $Al_6(Cu,Fe,Mn)$ [8, 24, 35, 36]. The former particles are typically smaller in size (as a rule, ≤4 μm) and regular in shape, whereas the latter are irregularly shaped and coarser (≥10 μm) [8, 24, 35, 36]. When present on the surface of the alloy, particles of both types impair the resistance of AA2024 to electrochemical corrosion [35, 36]. In connection with this, our focus in this study was on the nucleation and growth of PCCs on the surfaces of such intermetallic particles and the alloy matrix, which consists, for the most part, of a solid solution between Al and Cu (with trace amounts of Mg).

Figures 2a and 2b show SEM micrographs of two regions on the surface of AA2024 after treatment for 1 min. Comparison of the Al–Cu–Mg particle in Fig. 2a with the alloy matrix in Fig. 2b leads us to assume that, during treatment for 1 min, the coating was more likely to grow on the surface of the particle than on the alloy matrix. Al–Cu–Fe–Mn particles (not shown in Fig. 2) were also topographically distinct from the matrix, which suggests either slower dissolution of the particles in the alkaline solution or preferential growth of the PCC on their surfaces.

Figure 2c shows local Auger electron spectra of the regions marked in Figs. 2a and 2b. It is well seen that, after 1 min of treatment, a slight amount of Mn is present on the Al–Cu–Mg particle, whereas the spectrum of the region on the surface of the matrix (Fig. 2c, spectrum *2*) shows no Mn signal. Note that the Al sig-

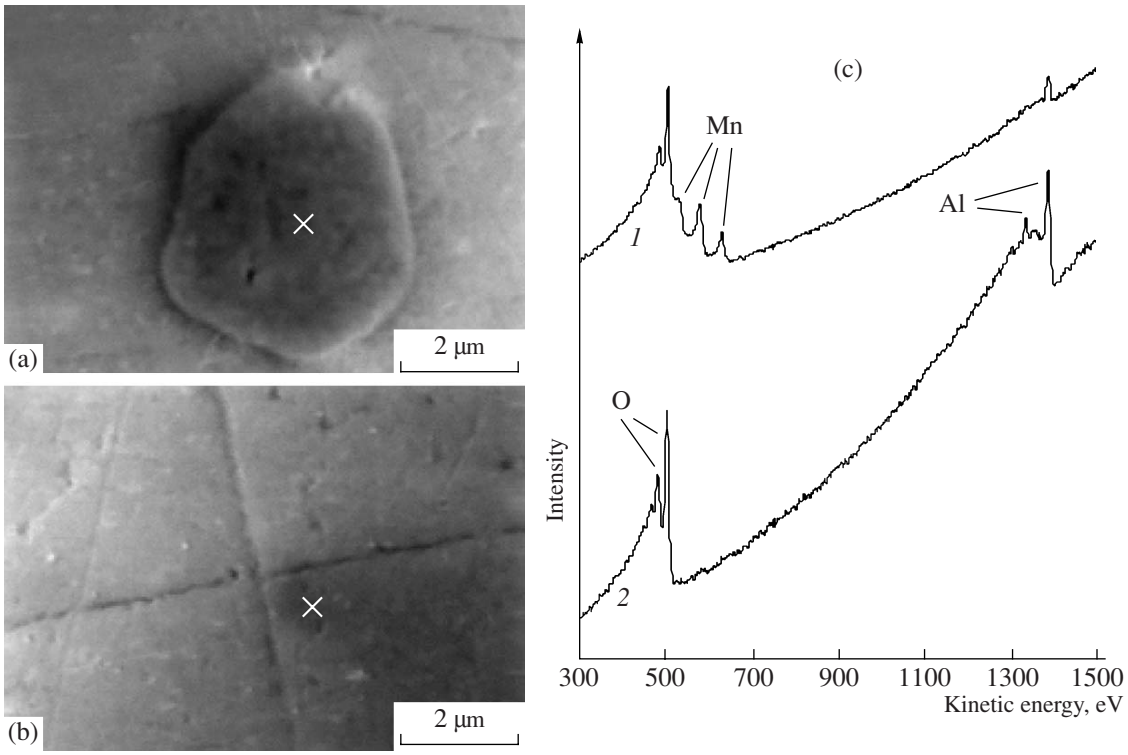

Fig. 2. SEM micrographs of (a) an Al–Cu–Mg particle and (b) the alloy matrix on the surface of an AA2024 sample treated at room temperature for 1 min; (c) local Auger electron spectra of the regions marked in panels (*1*) a and (*2*) b.

nals from the matrix are markedly stronger than those from the surface of the Al–Cu–Mg particle (Fig. 2c). The reason for this is that the PCC shields the Al atoms in the particle and on its surface. The Auger electron spectra of the coatings on coarser Al–Cu–Fe–Mn particles were similar to spectrum *1* in Fig. 2c, but showed an additional, weak Fe signal, which allowed us to distinguish between different phases in the initial stage of permanganate treatment. The Auger electron spectra of the coatings may vary from particle to particle, but Fig. 2c well illustrates the inhomogeneous manganese oxide distribution over the surface of AA2024 treated for 1 min: whereas the second-phase particles are coated with a thin conversion permanganate layer, the major phase has no coating.

Auger analysis of the sample treated for 5 min revealed trace levels of Mn on the surface of the AA2024 matrix. Figure 3 shows SEM images of an Al–Cu–Mg particle (Fig. 3a) and the alloy matrix (Fig. 3b), and the Auger electron spectra of their surfaces (Fig. 3c) after 20 min of treatment. As seen in Fig. 3a, the intermetallic particles became even more topographically distinct from the alloy matrix. Spectrum *1* in Fig. 3c confirms that the PCC on the particle became thicker: the Al signal is almost indiscernible (cf. Figs. 2c and 3c). The alloy matrix also shows significant surface changes and becomes similar in morphology to the PCCs described by Danilidis et al. [19]. Spectrum *2* in Fig. 3c attests to a significant amount of Mn on the surface of the matrix. At the same time, the presence of polishing scratches and the considerable intensity of the Al peak (Fig. 3c, spectrum *2*) indicate that the coating is far thinner than that on the surface of the intermetallic particles. Thus, Auger analysis results demonstrate that trace levels of PCCs appear on the surface of the major phase after 5 min of treatment at room temperature. After 20 min, the matrix is coated with a thin, uniform permanganate conversion layer, whereas the coating on the particles is notably thicker.

The above conclusions drawn from the Auger analysis data agree well with the XPS results. The metallic component of the Al 2*p* peak was only present in the spectra of the samples treated for 1 and 5 min. This leads us to conclude that the thickness of the PCC and the Al_2O_3 layer that may persist between the PCC and AA2024 substrate exceeds ≃5–10 nm at permanganate treatment times longer than 5 min. The Cu 2*p* peak was only observed at treatment times shorter than 5 min, which also lends support to the conclusion that the formation of a continuous PCC over the entire AA2024 surface requires at least ≃10 min. Since the XPS probing depth is ≤10 nm, a continuous PCC of this thickness will shield both Al and Cu in the bulk and on the surface of the AA2024 substrate.

Final stage of growth and defects in the coatings. Figure 4a shows a SEM micrograph (at a relatively low magnification) of the AA2024 surface after treatment for 30 min at room temperature. The intermetallic par-

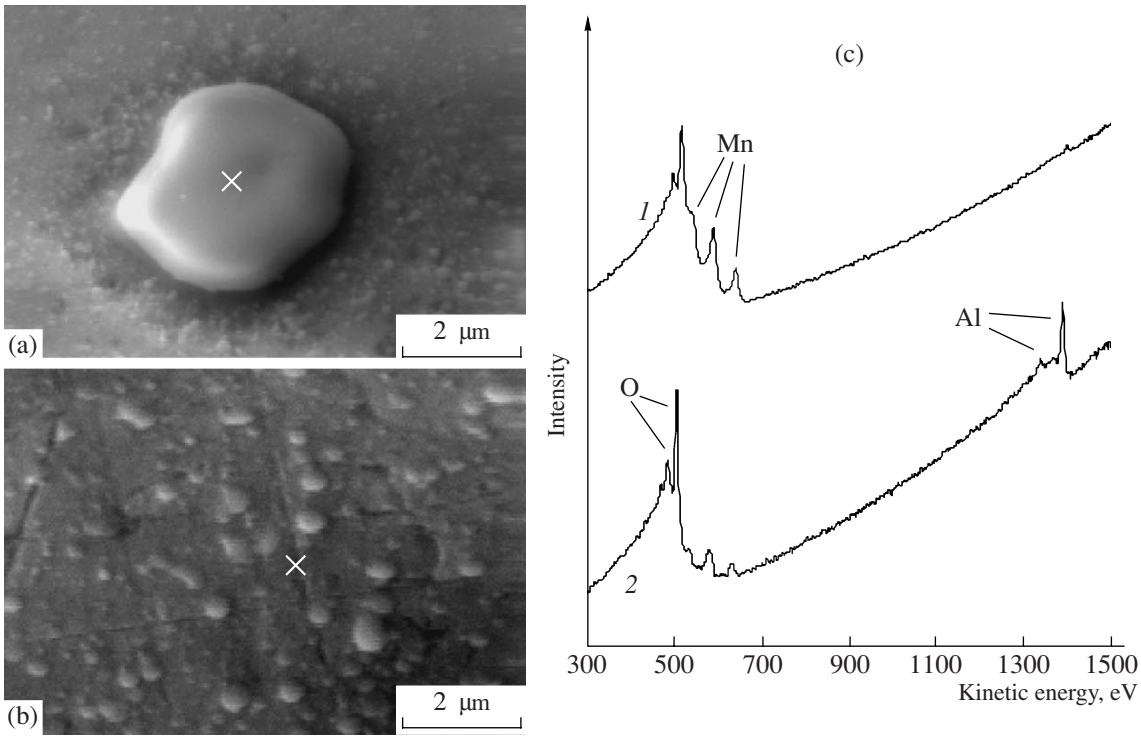

Fig. 3. SEM micrographs of (a) an Al–Cu–Mg particle and (b) the alloy matrix on the surface of an AA2024 sample treated for 20 min; (c) local Auger electron spectra of the regions marked in panels (*1*) a and (*2*) b.

ticles (marked by arrows) are seen to be coated with a rather thick permanganate conversion layer. The alloy matrix is covered with a thin PCC, but the polishing-induced scratches is well seen (arrow at the right of the micrograph). SEM results for longer $KMnO_4$ treatment times attest to further PCC growth over the entire alloy surface (Figs. 4b–4d). Thus, no qualitative changes occur during further PCC growth.

Figures 4b–4d show higher magnification SEM images which illustrate a typical surface morphology of the sample treated at room temperature for 150 min. The alloy matrix is seen to be uniformly coated (Fig. 4b). The Al–Cu–Fe–Mn (Fig. 4c) and Al–Cu–Mg (Fig. 4d) particles presumably have thick coatings. In contrast to the early stages of PCC growth (Figs. 2, 3, 4a), no polishing-induced scratches are seen on the surface of the alloy matrix (Fig. 4b). The coatings on most of the Al–Cu–Fe–Mn particles (Fig. 4c) have cracks, which developed, most likely, during drying because of the large thickness of the PCC. The present data are insufficient to conclude that the PCCs on the coarser particles are thicker than those on the Al–Cu–Mg particles, in which no cracks were detected (Fig. 4d). It seems, therefore, likely that the development of cracks in the coatings on the larger particles (containing Fe and Mn) is associated with their large size and irregular shape. Note that we also observed another type of defect: cracks along the perimeter of some particles (Fig. 4d). Such cracks are probably due to the difference in thickness between the coatings on the particle and surrounding alloy matrix or to the fact that, during electrochemical deposition of PCCs, the matrix adjacent to a cathodic particle dissolves more rapidly [8, 24].

Since thicker coatings are more insulating, and the probing depth is limited to ≃10 nm, local Auger electron spectroscopy is ineffective in analyzing PCCs in the later stages of growth. For this reason, to assess the local thickness of PCCs, we used local EDS measurements with a sampling size of ≃1 μm. Assuming that the PCCs on both the alloy matrix and intermetallic particles are chemically homogeneous, we suppose that the atomic ratio of Mn to the sum of the other major components of AA2024 (Mn/ΣM, M = Al, Cu, Mg, Fe) can be used to compare the thicknesses of the PCC above different microstructural constituents of the alloy surface. The table lists the Mn/ΣM values for the matrix and particles shown in Figs. 4b–4d. It is well seen that the Mn content of the coatings on the intermetallic particles far exceeds that on the matrix. The low values of the atomic ratio are due to the relatively large probing depth (1 μm). Thus, the EDS results lend support to the assumption inferred from SEM data that the PCCs on intermetallic particles are much thicker.

In addition, the proposed approach made it possible to reveal a very uniform manganese(IV) oxide distribution over the matrix surface at treatment times of 60 min or longer. The Mn/ΣM ratio in the sample kept

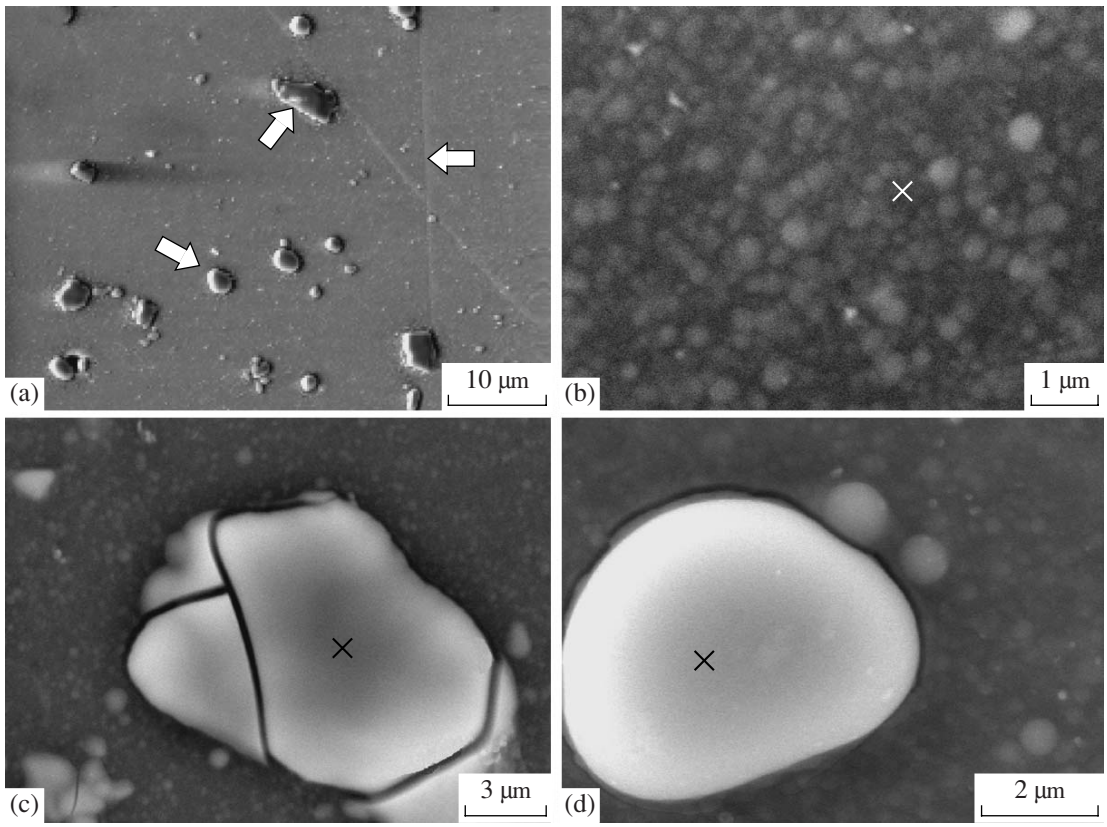

Fig. 4. SEM micrographs of AA2024 samples treated at room temperature for (a) 30 and (b–d) 150 min; (a) well-coated Al–Cu–Mg particles (smaller) and Al–Cu–Fe–Mn particles (larger); the arrow at the right of the micrograph marks a polishing scratch; (b) evenly coated matrix; (c) Al–Cu–Fe–Mn and (d) Al–Cu–Mg particles with thick PCCs.

in the solution for 90 min was very close to 0.008 throughout the alloy surface. Treatments of AA2024 for 150 and 210 min increased this ratio only slightly, to 0.009–0.01, thereby lending support to the conclusion that the PCC stops growing after ≃150 min of treatment.

The Mn/ΣM ratio measured above intermetallic second-phase particles was found to widely scatter, probably because the deposition rate depended on the particle size and electrochemical activity. For example, in the sample treated for 90 min, the ratio of Mn/ΣM above the particles to that above the matrix ranged from ≃2 (small particles) to ≃25 (large particles). In the samples treated for 150 and 210 min, this ratio varied from ≃3 to ≃30. This attests to a continuous PCC growth above both the alloy matrix and second-phase particles.

As seen in Figs. 4c and 4d, most defects in the PCC are concentrated around large intermetallic particles. These are cracks in the thick coatings on the irregularly shaped Al–Cu–Fe–Mn particles (Fig. 4c) and peripheral cracks at the particle–matrix interfaces, more common around large Al–Cu–Mg particles (Fig. 4d). Both types of cracks seem to develop during drying of the coatings. The PCC on the surface of the major phase of the alloy (Fig. 4b) is rather uniform in morphology and has no well-defined traces of defects or cracks, which fits well with the smaller thickness of the PCC in this region. It is, therefore, reasonable to assume that it is the high cathodic activity of second-phase particles in AA2024 (which contain Cu, a more noble element compared to Al), well documented in the literature [5, 24, 35, 36], which is responsible for the formation of the defects in question. This assumption is consistent with the approach patented by Bibber [15–18] to the protection of various Al alloys. To achieve effective corrosion protection of Cu- or Zn-rich alloys, including AA2024, an additional process step is necessary—treatment in a silicate solution. This step is intended to block the cracks and defects developing during PCC growth [16]. It is reasonable to expect that alloys that are poorer in Cu and Zn contain lower concentrations of large intermetallic second-phase particles. This, in turn, must reduce the defect density in PCCs, as observed in practice: such alloys require no treatment in silicate solutions.

Temperature effect. The AA2024 samples treated for 3 min at 50 and 68°C were close in properties to the samples treated at room temperature for 90 and 210 min, respectively. SEM examination of those samples showed that they were similar in surface morphology. The Mn/ΣM ratio (evaluated from EDS data) in the sample prepared at 68°C was rather close to the values

Mn/ΣM ratios extracted from EDS measurements for the sample treated in a permanganate solution for 150 min

Analyzed area*	Mn/ΣM
Fig. 4b	0.009
Fig. 4c	0.11
Fig. 4d	0.07

* The analyzed area is marked by a cross in the micrograph.

in the table, and the samples prepared at room temperature (90 min) and 50°C (3 min) were also almost identical in Mn/ΣM. Thus, treatment of AA2024 in the temperature range 25–68°C produces morphologically similar conversion coatings. The main effect of raising the deposition temperature is to increase the growth rate, in accordance with earlier reports [16–18].

At room temperature, PCC formation reaches completion in ≃150 min, whereas at elevated temperatures (50–68°C) the growth rate is faster, and the PCC stops growing after several minutes. This coating time is slightly longer than the one reported by Bibber [15–17] (≃1 min at 68°C), which may be due to differences between the procedures used for polishing and sample preparation before immersing the Al plates in the reaction solution. Since the thickness and nature of the oxide layer strongly depends on the sample preparation procedure, one would expect a variation in the rate of PCC growth, which involves dissolution of the surface oxide.

CONCLUSIONS

As in the case of chromate coatings [5, 7, 8, 24], the growth of PCCs on aluminum alloy 2024 begins on the surface of intermetallic second-phase particles, which display cathodic activity with respect to the major phase of the alloy. At room temperature, traces of a coating on the surface of the major phase appear after ≃5 min of keeping the alloy in an alkaline $KMnO_4$ solution. After ≃150 min of room-temperature treatment, the growth rate drops, and the coating stops growing. In the temperature range 50–68°C, the process takes ≃3 min to reach completion, and the resulting coatings are very close in surface morphology and thickness to the coatings grown at room temperature.

The major component of the coatings is hydrated MnO_2, in accordance with earlier reports. The major impurities in the coatings are Mg, K, and Na, whereas the amounts of Al, Cu, and B are insignificant. Since the amount of permanganate ions in our coatings (based on manganese(IV) oxide) is also insignificant, they are unlikely to be capable of active corrosion protection, in contrast to some other conversion coatings.

In our samples, the coating on the second-phase particles is always markedly thicker, which is, most likely, responsible for the formation of defects (cracks) in the coating near such particles.

REFERENCES

1. Hughes, A.E., Taylor, R.J., and Hinton, B.R.W., Chromate Conversion Coatings on 2024 Al Alloy, *Surf. Interface Anal.*, 1997, vol. 25, no. 4, pp. 223–234.
2. Hinton, B.R.W., Corrosion Prevention and Chromates: The End of an Era?: Part 1, *Met. Finish.,* 1991, vol. 89, no. 9, pp. 55–59.
3. Hinton, B.R.W., Corrosion Prevention and Chromates: The End of an Era?, *Met. Finish.*, 1991, vol. 89, no. 10, pp. 15–20.
4. Kending, M.W. and Buchheit, R.G., Corrosion Inhibition of Aluminum and Aluminum Alloys by Soluble Chromates, Chromate Coatings, and Chromate-Free Coatings, *Corrosion*, 2003, vol. 59, no. 5, pp. 379–400.
5. Brown, G.M. and Kobayashi, K., Nucleation and Growth of a Chromate Conversion Coating on Aluminum Alloy AA2024-T3, *J. Electrochem. Soc.*, 2001, vol. 148, no. 11, pp. B457–B466.
6. Xia, L. and McCreery, R.L., Chemistry of a Chromate Conversion Coating on Aluminum Alloy AA2024-T3 Probed by Vibrational Spectroscopy, *J. Electrochem. Soc.,* 1998, vol. 145, no. 9, pp. 3083–3089.
7. Kulinich, S.A., Akhtar, A.S., Susac, D., et al., Surface Science Studies of the Effect of Al Alloy Microstructure on the Formation of Chromate Coatings, *Mater. Sci. Forum*, 2006, vols. 519–521, pp. 621–628.
8. Kulinich, S.A., Akhtar, A.S., Susac, D., et al., On the Growth of Conversion Chromate Coatings on 2024-Al Alloy, *Appl. Surf. Sci.,* 2007, vol. 253, no. 6, pp. 3144–3153.
9. Smit, M.A., Sykes, J.M., Hunter, J.A., et al., Titanium Based Conversion Coatings on Aluminium Alloy 3003, *Surf. Eng.,* 1999, vol. 15, no. 5, pp. 407–410.
10. Buchheit, R.G., Mamidipall, S.B., Schmutz, P., and Guan, H., Active Corrosion Protection in Ce-Modified Hydrotalcite Conversion Coatings, *Corrosion*, 2002, vol. 58, no. 1, pp. 3–14.
11. Decroly, A. and Petitjean, J.-P., Study of the Deposition of Cerium Oxide by Conversion on to Aluminium Alloys, *Surf. Coat. Technol.*, 2005, vol. 194, no. 1, pp. 1–9.
12. Guan, H. and Buchheit, R.G., Corrosion Protection of Aluminum Alloy 2024-T3 by Vanadate Conversion Coating, *Corrosion*, 2004, vol. 60, no. 3, pp. 284–296.
13. Khramov, A.N., Voevodin, N.N., Balbyshev, V.N., and Mantz, R.A., Sol–Gel-Derived Corrosion-Protective Coatings with Controllable Release of Incorporated Organic Corrosion Inhibitors, *This Solid Films*, 2005, vol. 483, nos. 1–2, pp. 191–196.
14. Zheludkevich, M.L., Serra, R., Montemor, M.F., et al., Corrosion Protective Properties of Nanostructured Sol–Gel Hybrid Coatings to AA2024-T3, *Surf. Coat. Technol.*, 2006, vol. 200, no. 9, pp. 3084–3094.
15. Bibber, J.W., US Patent 4 711 667, 1987.
16. Bibber, J.W., US Patent 4 755 224, 1988.
17. Bibber, J.W., US Patent 4 878 963, 1989.

18. Bibber, J.W., Chromate-Free Conversion Coatings for Aluminum, *Plat. Surf. Finish.*, 2003, vol. 90, no. 3, pp. 40–43.
19. Danilidis, I., Sykes, J.M., Hunter, J.A., and Scamans, G.M., Manganese Based Conversion Treatment, *Surf. Eng.*, 1999, vol. 15, no. 5, pp. 401–405.
20. Danilidis, I., Hunter, J.A., Scamans, G.M., and Sykes, J.M., Effects of Inorganic Additions on the Performance of Manganese-Based Conversion Treatments, *Corros. Sci.*, 2007, vol. 49, no. 3, pp. 1557–1569.
21. Buchheit, R.G., Cunningham, M., Jensen, H., et al., A Correlation between Salt Spray and Electrochemical Impedance Spectroscopy Test Results for Conversion-Coated Aluminum Alloys, *Corrosion*, 1998, vol. 54, no. 1, pp. 61–72.
22. Mikhailovskii, Y.N. and Berdzenishvili, G.A., Influence of pH on Electrochemical and Corrosion Behaviour of Aluminum in Media Containing Oxo Anions of the Oxidizing Type, *Prot. Met.*, 1985, vol. 21, no. 6, pp. 758–762.
23. Srinivasan, P.B., Sathiyanarayanan, S., Marikkannu, C., and Balakrishnan, K., A Non-chromate Chemical Conversion Coating for Aluminum Alloys, *Corros. Prev. Control*, 1995, vol. 42, no. 2, pp. 35–37.
24. Campestrini, P., Terryn, H., Vereecken, J., and de Wit, J.H.W., Chromate Conversion Coatings on Aluminum Alloys: II. Effect of the Microstructure, *J. Electrochem. Soc.*, 2004, vol. 151, no. 6, pp. B359–B369.
25. Nylund, A., Chromium-Free Conversion Coatings for Aluminum Surfaces, *Alum. Trans.*, 2000, vol. 2, no. 1, pp. 121–137.
26. Umehara, H., Terauchi, S., and Takaya, M., Structure and Corrosion Behaviour of Conversion Coatings on Magnesium Alloys, *Mater. Sci. Forum,* 2000, vols. 350–351, pp. 273–282.
27. Umehara, H., Takaya, M., and Terauchi, S., Chrome-Free Surface Treatments for Magnesium Alloy, *Surf. Coat. Technol.,* 2003, vols. 169–170, pp. 666–669.
28. Takaya, M., Produce of Manganese-Type Chemical Conversion Coatings for Magnesium Alloys and Their Corrosion Resistance, *Jpn. Inst. Light Met.*, 1995, vol. 45, no. 12, pp. 713–718.
29. Zhao, M., Wu, S.S., Luo, J.R., et al., A Chromium-Free Conversion Coating of Magnesium Alloy by a Phosphate–Permanganate Solution, *Surf. Coat. Technol.*, 2006, vol. 200, nos. 18–19, pp. 5407–5412.
30. Chong, K.Z. and Shih, T.S., Conversion-Coating Treatment for Magnesium Alloys by a Permanganate–Phosphate Solution, *Mater. Chem. Phys.*, 2003, vol. 80, no. 1, pp. 191–200.
31. Umezawa, Y. and Reilley, C.N., Effect of Argon Bombardment of Metal Complexes and Oxides Studied by X-ray Photoelectron Spectroscopy, *Anal. Chem.,* 1978, vol. 50, no. 9, pp. 1290–1295.
32. Audi, A.A. and Sherwood, P.M.A., Valence-Band X-ray Photoelectron Spectroscopic Studies of Manganese and Its Oxides Interpreted by Cluster and Band Structure Calculations, *Surf. Interface Anal.,* 2002, vol. 33, no. 15, pp. 274–282.
33. Oku, M., Matsuta, H., and Wagatsuma, K., Removal of Inelastic Scattering Parts from the Mn 2*p* X-ray Photoelectron Spectrum for Potassium Permanganate by a Deconvolution Method Using the K 2*p* and O 1*s* Spectra As a Response Function, *Bunseki Kagaku*, 1997, vol. 46, no. 9, pp. 703–709.
34. Oku, M., X-ray Photoelectron Spectra of $KMnO_4$ and K_2MnO_4 Fractured In Situ, *J. Electron Spectrosc. Relat. Phenom.*, 1995, vol. 74, no. 2, pp. 135–148.
35. Buchheit, R.G., Grant, R.P., Hlava, P.F., et al., Local Dissolution Phenomena Associated with *S* Phase (Al_2CuMg) Particles in Aluminum Alloy 2024-T3, *J. Electrochem. Soc.*, 1997, vol. 144, no. 8, pp. 2621–2628.
36. Kolics, A., Besing, A.S., and Wieckowski, A., Interaction of Chromate Ions with Surface Intermetallics on Aluminum Alloy 2024-T3 in NaCl Solutions, *J. Electrochem. Soc.*, 2001, vol. 148, no. 8, pp. B322–B331.